RADC-TR-72-110
Technical Report
14 April 1972

BLEACHABLE ABSORBER LASER AMPLIFIER AND DETECTOR (BALAD)

Polytechnic Institute of Brooklyn

Sponsored By
Advanced Research Projects Agency
ARPA Order No. 1279
Amendment No. 2

Rome Air Development Center
Air Force Systems Command
Griffiss Air Force Bose, New York

Reproduced by
NATIONAL TECHNICAL
INFORMATION SERVICE
U S Department of Commerce
Springfield VA 22151

DISCLAIMER NOTICE

THIS DOCUMENT IS THE BEST QUALITY AVAILABLE.

COPY FURNISHED CONTAINED A SIGNIFICANT NUMBER OF PAGES WHICH DO NOT REPRODUCE LEGIBLY.

UNCLASSIFIED

Security Classification

DOCUMENT CONTROL DATA - R & D

(Security classification of title, body of abstract and indexing annotation must be entered when the overall report is classified)

1. ORIGINATING ACTIVITY *(Corporate author)*
Polytechnic Institute of Brooklyn, Dept. of Electrical Engineering and Electrophysics, Long Island Graduate Center, Route 110, Farmingdale, New York 11735

2a. REPORT SECURITY CLASSIFICATION
Unclassified

2b. GROUP

3. REPORT TITLE
Bleachable Absorber Laser Amplifier and Detector (BALAD)

4. DESCRIPTIVE NOTES *(Type of report and inclusive dates)*
Scientific Semi-Annual. 18 Nov 70 through 17 Nov 71.

5. AUTHOR(S) *(First name, middle initial, last name)*
Gordon Gould and James T. LaTourrette

6. REPORT DATE	7a. TOTAL NO. OF PAGES	7b. NO. OF REFS
April 14, 1972	40	19

8a. CONTRACT OR GRANT NO	9a. ORIGINATOR'S REPORT NUMBER(S)
F30602-71-C-0024	PIBEP-72-106
b. PROJECT NO.	
c.	9b. OTHER REPORT NO(S) *(Any other numbers that may be assigned this report)*
d. ARPA Order No. 1279, Amendment No. 2	RADC-TR-72-110

10. DISTRIBUTION STATEMENT
Approved for public release; distribution unlimited.

11. SUPPLEMENTARY NOTES	12. SPONSORING MILITARY ACTIVITY
Monitored by Mr. William Quinn, 315-330-3030 RADC (OCTM-1) GAFB/NY 13440	Advanced Research Projects Agency Washington, D.C. 20301

13. ABSTRACT

A detailed feasibility and design study has been made on the wide-angle, low noise BALAD receiver (Bleachable Absorber Laser Amplifier and Detector). Expressions have been derived for the achievable field-of-view, maximum gain and other specifications in terms of the dimensions and the measurable properties of the laser and absorber gases. Virtually error free detection is assured for signal pulses >100 photons.

A figure-of-merit has been measured for several absorber gases screened from the literature. BALAD receivers with 4000 resolution element field-of-view are feasible using SF_6 with a CO_2 amplifier at 10.6 um and Xe with Xe at 3.5um. The use of the latter is recommended for the experimental test of the BALAD receiver. Two compact absorber configurations have been considered and will be further investigated. Application is to optical radar and to optical communications where signal direction is uncertain.

DD FORM 1 NOV 65 1473

UNCLASSIFIED

Security Classification

14. KEY WORDS	LINK A		LINK B		LINK C	
	ROLE	WT	ROLE	WT	ROLE	WT
Laser amplifier						
Laser receiver						
Laser detector						
CO_2 laser						
Xenon laser						
Absorber						
Bleachable absorber						
Saturable absorber						
Gaseous absorber						
Optical filter						
Sulfur hexafluoride						
Optical waveguide						
Optical radar						
Optical communications						
Wide-angle detector						
Low-noise detector						
Coherent detector						
Narrow band filter						
Spatial filter						

BLEACHABLE ABSORBER LASER AMPLIFIER AND DETECTOR (BALAD)

Gordon Gould
James T. LaTourrette

Contractor: Polytechnic Institute of Brooklyn
Contract Number: F30602-71-C-0024
Effective Date of Contract: 18 November 1970
Contract Expiration Date: 17 November 1971
Amount of Contract: $103,268.00
Program Code Number: 0E20

Principal Investigators: G. Gould and
J. T. LaTourrette
Phone: 516 694-5500

Project Engineer: G. Gould
Phone: 516 694-5500

Contract Engineer: W. C. Quinn
Phone: 315 330-3030

Approved for public release;
distribution unlimited.

This research was supported by the Advanced Research Projects Agency of the Department of Defense and was monitored by William Quinn, RADC (OCTM), GAFB, NY 13440 under contract F30602-71-C-0024.

FOREWORD

This technical report was prepared by Polytechnic Institute of Brooklyn under Contract F30602-71-C-0024. It describes work performed at the Long Island Graduate Center, Farmingdale, N.Y.. The principle investigators are Dr. Gordon Gould and Dr. James LaTourrette. Dr. Gould is also project engineer.

The Air Force Program Monitor is William C. Quinn, OCTM.

PUBLICATION REVIEW

This technical report has been reviewed and is approved.

William C. Quinn

RADC Project Engineer

TABLE OF CONTENTS

LIST OF FIGURES

LIST OF TABLES

1.0 Summary.

1.1 Objective.

The objective of the subject contract is the investigation of Saturable Absorbers and their application to wide-angle, low-noise laser receivers.

1.2 Background.

The combination of a Bleachable Absorber Laser Amplifier and a Detector (BALAD) as a receiver may have advantages over optical heterodyne or direct detection receivers, in the area of field of view, detectivity, and bandwidth. In the BALAD concept the signal beam is amplified along with spontaneous emission from excited molecules in a laser pre-amplifier. The gaseous absorber is designed to saturate at an average intensity above the amplified spontaneous emission. Thus, the spontaneous emission and other background light is absorbed. The bleachable or saturable absorbing gas acts as an optical squelch suppressing the background radiation which does not coincide with the signal beam in direction, polarization, frequency and time. In addition, the signal beam of somewhat higher intensity is focused down on the absorber, "burns a hole" in it, and passes through with relatively little attenuation. Only light which is spatially coherent with the signal gets through to the detector.

Two possible configurations for the receiver are shown schematically in Figures 1 and 2. The operation of the receiver is described in more detail in Sections 2.1.1 and 2.1.2.

1.3 Plan.

In the subject one-year contract, the scope is limited to two tasks (line item A001):

Task 4.1.1: Screen the potentially useful absorbers in the 10.6 μ and 3-5 μ spectral ranges and measure the relevant properties of the most promising gases.

Task 4.1.3: Extend the feasibility and design study of the BALAD receiver.

1.4 Technical Problems, Methodology, and Results.

This report contains the detailed results of Task 4.1.3 with which receiver performance can be predicted and physical design constants outlined. It also contains a summary of the results of Task 4.1.1 - that is, the important measured properties of the best absorbers and specifications for two embodiments of the receiver. It thus

Fig. 1(a) - BALAD receiver. Absorber becomes transparent at the focus and frequency of the signal beam.

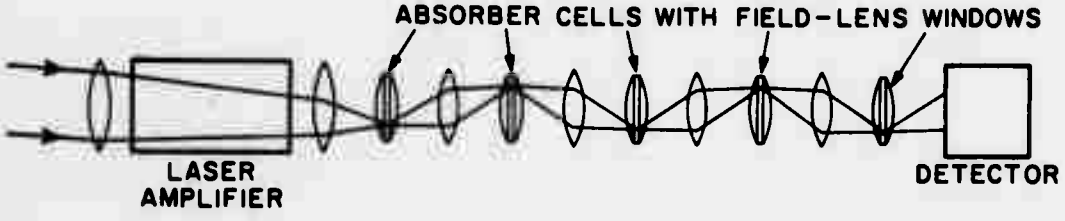

Fig. 1(b) - BALAD receiver with fine-focus multi-stage absorber required for gas with low attenuation and high saturation intensity.

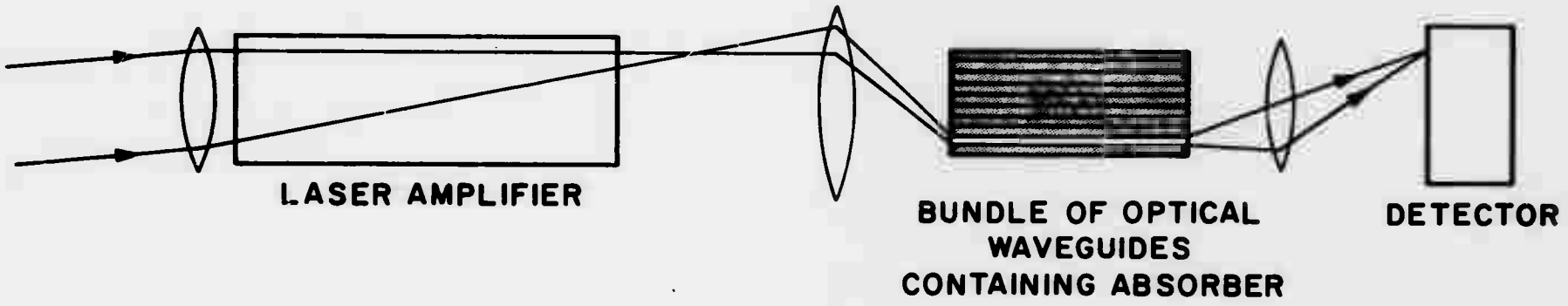

Fig. 2 - Alternative BALAD arrangement to that of Fig. 1. Periodic refocusing through absorber is unnecessary if light is confined in a waveguide.

provides the basis for decisions on the future course of the program.

The final technical report will contain a summary of Task 4.1.3 and a detailed discussion of Task 4.1.1. It will thus serve as an appendix to the First Technical Report.

1.4.1 Feasibility and Design Study

The most important questions addressed by this study are: (a) How large a field-of-view through the receiver is allowed by the actual characteristics of the best absorbers and by the technological and economic limitations on fabrication of the absorber configuration? (b) How big is the minimum signal which can be detected with satisfactory error rates?

(a) The principle advantage of the BALAD receiver over either direct detection or optical heterodyne detection of a radar or communication signal is this: BALAD can detect with maximum sensitivity a signal from any arbitrary direction in a sizeable field-of-view instead of having to close down the field-of-view to a single diffraction limited cone or resulution element.[1] It is therefore important to ask how large this field may be. In Section 2.1.1, it is shown that the maximum field-of-view through the receiver is given by

$$\Omega_v \cong \text{constant} \times \frac{sF_M}{[\varphi\lambda^2]} \qquad (1.4.1\text{-}1)$$

where $F_M \equiv$ figure-of-merit for the absorbing gas.

$\varphi,\lambda \equiv$ branching ratio, wavelength characteristic of the laser amplifier medium.

$s \equiv$ number of stages in which the amplified signal is refocused down through the absorber.

The number of stages, s, is inversely proportional to the area of the diffraction limited focused spot in the absorber. Thus, in addition to the limitations imposed by the laser and absorber media, Ω_v is limited by the economically acceptable length of a lens train in the absorber region, or by the smallness of technically feasible optical waveguides for confining the focused signal beam.

The losses to be expected in optical waveguides, and the feasibility of fabricating a bundle of such guides are examined in Section 2.1.2.

The awkwardness and bulkiness of the long lens train shown in Fig. 1-b may be avoided by a recently conceived modification of the free-focus configuration. The

large lenses are replaced "fly's eye" lenses covering the field of possible signal spots. A series of such compound lenses in the absorber then prevents the focused beam from respreading. Thus the length of the train is collapsed to the actual required path length through the abosrber (perhaps 2 meters). Such lenses may be economically molded from the infrared transmitting Irtran materials. The "fly's eye" configuration will be discussed in the Final Technical Report.

A second advantage of the BALAD receiver is that the absorber acts as a spectral filter which passes only the narrow signal band wherever it may fall. It is notable that the width of the signal band does not affect the achievable field-of-view. It does enter into other design parameters which may be calculated from the developed theory: path length through absorber, maximum output power, focused spot size, etc.

(a) The no-detection and false-detection error rates, other than those generated by circuit failure, arise at the input to the amplifier from photon fluctuations in the signal pulse relative to the spontaneous emission or "noise" pulse. It is shown in Section 2.1.3 that the error rates primarily depend on the size of the average signal pulse and are little affected by other design considerations. The error rates rapidly become vanishingly small for signal pulses larger than 100 photons.

1.4.2 Investigation of Gaseous Absorbers

The figure-of-merit for absorbing gases,

$$F_M \equiv \left[\frac{\alpha_o B}{I_s}\right] \qquad (1.4.2\text{-}1)$$

is defined in Section 2.1.1. It is computed from measured values of the absorption coefficient, α_o, the saturation intensity, I_s, and the collision induced saturation bandwidth, B.

Two types of gaseous absorbers have been investigated:

(a) Unexcited molecules which absorb via vibration-rotation transitions within the well populated electronic ground state. The CO_2 laser transitions are of this type. These transitions are generally weak. The only absorbing transitions which have been found to overlap CO_2 laser transitions are of this type. The literature has been searched and a list of 75 potential absorbers in the 10.6μ meter and 3-5μm bands has been compiled. Rough absorption measurements reduced the list to 2 likely candidates. The figures-of-merit, F_M, were measured using apparatus designed and built in part under the contract. The best of these was sulfur hexafluoride (SF_6) with $F_M = 3 \times 10^5$ meter/joules (See Table 2.2.1-1). An available review of vibration-rotation transitions in general suggests that a higher value of F_M is not likely to be found.

(b) Atoms which absorb via "allowed" transitions between electronic states excited or populated by an electric discharge. The high gain, $\lambda = 3.5\,\mu m$ laser transition in xenon (Xe) is of this type. It can be made absorbing by over-driving the discharge. The figure-of-merit was measured to be $F_M = 5 \times 10^7 m/j$. It is likely that this can be further improved by variation of measurement conditions.

1.4.3 BALAD Receiver Characteristics.

Examples of feasible receiver specifications have been calculated for the CO_2-SF_6 and Xe-Xe combinations. These are presented in Table (2.2.2-1). The Xe-Xe design can be economically tested in 1972. Briefly summarized, the CO_2-SF_6 design would have a field-of-view of 4000 resolution elements (0.5 degree diameter) and an essentially error-free maximum peak signal pulse output power of 0.2 watts at the detector or optical signal processor. The unfolded amplifier length would be 10 meters and the diameter 10 cm. Either the "fly's eye" or optical waveguide absorber configurations would be 2 meters long.

An Xe-Xe BALAD utilizing the fly's eye configuration could have a field-of-view of 400,000 resolution elements of 5^o angular diameter (equivalent to a commercial television raster. The state-of-the-art Xe laser transmitter average power is 1 watt at $\lambda = 3.5\mu m$.

1.5 Implications for DoD.

A BALAD receiver for $10.6\mu m$ CO_2 laser signals with the specifications referred to above is feasible for application in an optical radar. The usefulness would be to detect a target of uncertain position. For example, the receiver could be remote from the transmitter. It could also sensitively receive several separated signals simultaneously, or even an entire image.

A BALAD receiver utilizing xenon gas could function in a shorter range but higher resolution optical radar in comparison to the CO_2 system. This wide-angle receiver also could be utilized in a lightweight secure communication system.

1.6 Implications for Further R&D.

(a) an experimental test of the BALAD receiver principle utilizing Xenon gas can be economically made and should be carried out in 1972.

(b) the "fly's eye" and optical waveguide absorber configurations should be further investigated with a view to determining:

1) How compact and economical the absorber design can be made.

2) How small can the focal spot be made (and therefore how large the field-of-view) without incurring undue losses.

(c) a computer search using an existing data bank should be carried out to see if an excited atomic absorber line overlaps a CO_2 laser line.

(d) an investigation should be made of techniques for filtering out spontaneous emission from all but the working CO_2 laser line.

2.0 Saturable Absorbers and the BALAD Receiver.

The objective of this research program is the "Investigation of Saturable (or Bleachable) Absorbers and their application to wide-angle, low-noise receivers." The spectral regions of interest are $\lambda = 10.6$ micrometer and $\lambda = 3\text{-}5$ μm.

The "engineering services for the development, design, test and analysis of the concept of a BALAD receiver" were initially limited to two tasks:

Task 4.1.1. A theoretical and experimental investigation of the essential properties of promising saturable gaseous absorbers (see Section 2.2 below).

Task 4.1.3. A feasibility and design study of the BALAD receiver (see Section 2.1).

Other tasks, including the experimental test of a BALAD receiver were postponed until positive results were obtained in the above (see Section 1.6).

2.1 Feasibility and Design Study of the BALAD Receiver.

Task 4.1.3. - calls for "refining and extending the theory for more effective design by taking into account the data and possible effects of the Investigation of Saturable Absorbers (Task 4.1.1). In particular, derive the necessary analytical expression(s) to determine performance, reliability, and cost estimates."

The desired analytic expressions have now been derived for the configuration proposed in Fig. 1 and the mode of operation of the BALAD receiver. This theory rests on the well-understood interactions between gaseous matter and radiation. The basic design equations (derived below) relate maximum possible field-of-view through the laser amplifier, the receiver dimensions, required attenuation of noise, and characteristics of amplifier and absorber gases. In particular, the possible field-of-view is related to a figure-of-merit for the absorber.

The BALAD receivers of greatest interest at present would utilize a CO_2 laser amplifier and a SF_6 bleachable absorber gas. It turns out in this case that to obtain sufficient noise attenuation and a useful field-of-view, the signal beam must be refocused through the absorber many times (as in Fig. 1-b). Quite recently it has been realized that such multistage refocusing may be obviated by the "optical waveguide" configuration shown in Fig. 2. Although this modification has not yet been thoroughly studied, preliminary analysis indicates that wall attenuation will not be excessive and fabrication should be feasible. If so, a larger field-of-view, a more compact device, and other advantages would ensue. Some considerations are discussed in Section 2.1.2.

2.1.1. Free Focus Configuration.

The proposed mode of operation of the BALAD receiver is as follows: The signal is focused through the laser amplifier down to a diffraction limited Fraunhofer spot in the saturable absorber. Spontaneous emission from a region near the input end of the amplifier (from the first "gain length," actually) is also amplified and falls on the absorber.

The minimum no-detection and false-detection error rates are determined at the input by the fluctuations in the signal pulse and in the accompanying spontaneous emission within the spatial mode and spectral band of the signal. (See Section 2.1.3.)

It turns out that, to achieve acceptable error rates, the signal power or pulse energy must be about 100 times or 20 dB greater than the spontaneous emission in the signal mode (or modes) and signal bandwidth. On the other hand, the spontaneous emission power or pulse energy in all modes is much larger than the detectable signal. Thus, the typical case is that depicted in Fig. 3.

One may think of the spatial modes as the various cones and focal spots which might be occupied by the signal beam. As many spatial modes pass through the amplifier as there are resolution elements in the field-of-view through the amplifier – perhaps 4000. In each spatial mode the spontaneous emission power is proportional to the bandwidth. If the gain bandwidth of a CO_2 laser line were ~20 times the signal bandwidth, the total spontaneous power in 1 spatial mode would be 20 times that within the signal bandwidth. Thus, the total spontaneous power impinging on the absorber might be 30 dB greater than the signal and 50 dB greater than the spontaneous emission coherent with the signal. It is this spontaneous emission in other spatial and frequency modes which the absorber is to block.

The signal must be amplified as much as possible in order to minimize its attenuation on passage through the partially saturated absorber in the focal spot. The maximum gain is limited by saturation of the laser medium by the amplified spontaneous emission to (see Section 2.1.4):

$$G_{max} = \left.\frac{I_{out}}{I_{in}}\right|_{max} \cong \frac{16L^2}{\varphi\psi D^2} \qquad (2.1.1\text{-}1)$$

or

$$G_{max} = \frac{4\pi}{\varphi\psi\sigma_v} \qquad (2.1.1\text{-}2)$$

where

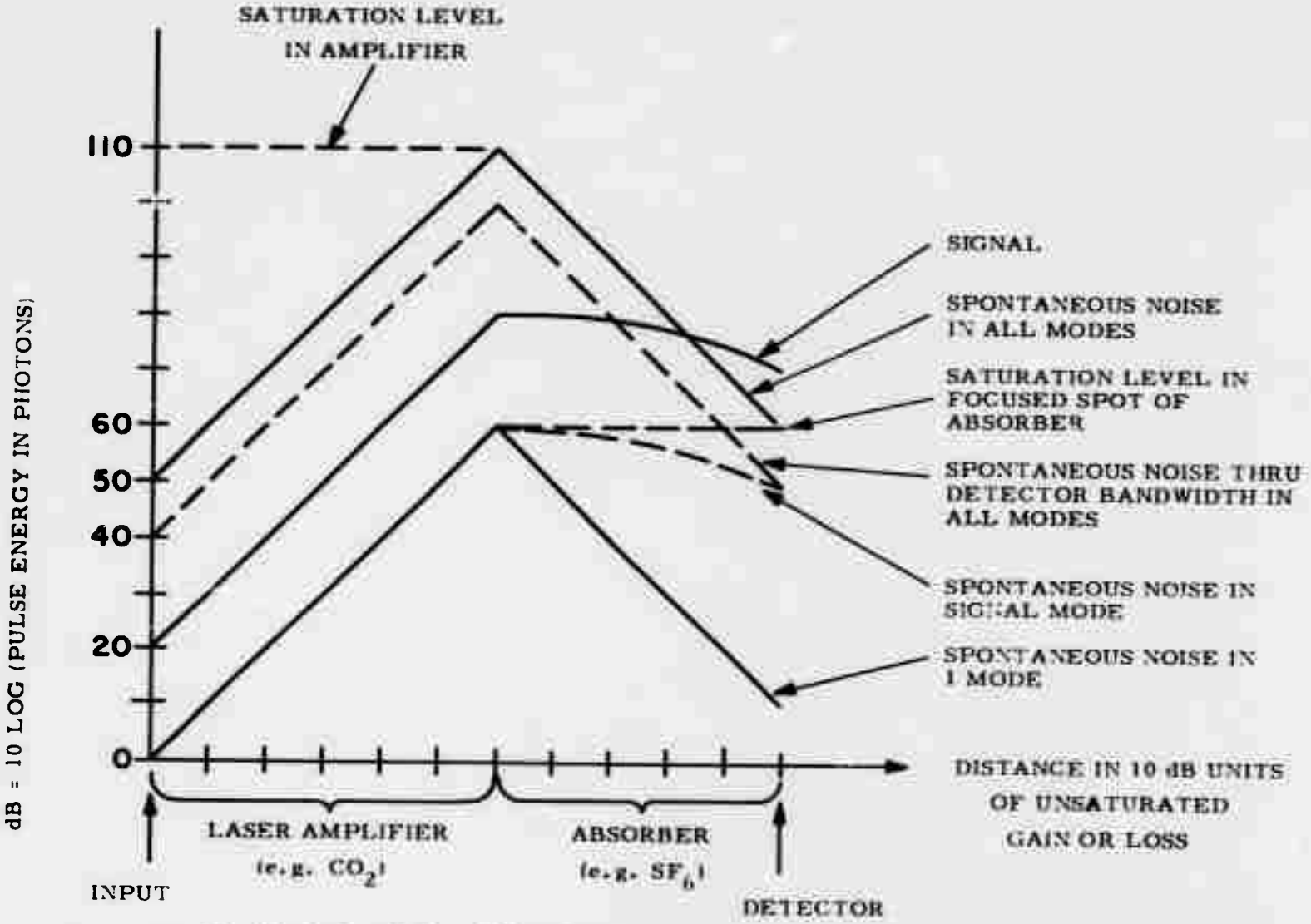

Fig. 3 - Typical evolution of signal and noise pulse energies on passing through the BALAD receiver. The spatial modes are cones leading to resolved focal spots. Post-detector bandwidth reduces the noise from its wideband value by $\sqrt{\frac{\text{signal-band}}{\text{amplifier band}}}$.

I = signal intensity

L = amplifier length

D = amplifier diameter

Ω_v = angular field of view through the amplifier (in steradians)

Ψ = Gain bandwidth narrowing factor which reduces the amplified spontaneous power

φ = Effective branching ratio of the laser transition which is inversely proportional to the saturation intensity.

That is, the maximum unsaturated gain (derived in Section 2.1.4) varies inversely with the field of view. This is because the number of modes and hence the amount of spontaneous power which can reach the ends of the amplifier is proportional to Ω_v.

The size of the focal spot must be adjusted so that the amplified spontaneous intensity equals the saturation intensity of the absorber. Then the spontaneous intensity is attenuated linearly on passage through the absorber:

$$[\text{dB (attenuation)}] = 10 \log_{10}\left[\frac{I_{in}}{I_{out}}\right]_{spont} = 4.34 \alpha_o \ell_a s \qquad (2.1.1\text{-}3)$$

where

α_o = unsaturated absorption coefficient

ℓ_a = path length through absorber near focal spot

s = number of absorber stages.

On the other hand, since the signal intensity, in its focal spot, is greater than the saturation intensity, the absorption coefficient is reduced to:

$$\alpha_s \frac{\alpha_o}{\sqrt{1 + I/I_s}} \qquad (2.1.1\text{-}4)$$

where I_s = saturation intensity of absorber.

Thus the signal is attenuated less rapidly than the amplified spontaneous power in other spatial modes. Equation (2.1.1-4) gives the correct dependence of α_s for an inhomogeneous (Doppler broadened) absorption line.[2] The high intensity reduces only that absorbing population difference with Doppler shift corresponding to the signal bandwidth.

The "depth of focus," ℓ_a, is the length of absorber near the "waist" of the focal spot. ℓ_a is limited by the requirement that the amplified spontaneous power be focused

into a small enough spot to just saturate the absorber as it enters (see Fig. 4). That is:

$$I_s \approx \frac{P_{spont}(1\ mode)}{\pi a_m^2} \qquad (2.1.1\text{-}5)$$

where

$$\pi a_m^2 = \text{focal spot area} \quad .$$

The hyperboloidal shape of the "waist" in the extended focal spot is well approximated by the confocal laser resonator theory of Boyd and Kogelnick if the signal beam is initially an undistorted plane wave.[3] The cross-sectional area of the beam in the absorber must never be much larger than the minimum spot area, since the signal intensity must remain well above the saturation intensity. If the maximum diffracted beam radius is (somewhat arbitrarily) limited to $a = 2a_m$, there it may be readily calculated that the path length,

$$\ell_a = 2\sqrt{3}\ \frac{\pi a_m^2}{\lambda} \qquad (2.1.1\text{-}6)$$

where λ = signal wavelength. If a longer value of ℓ_a is used, the signal pulse energy must be increased in proportion to ℓ_a^2.

The amplified spontaneous emission in one mode is given by[4]

$$P_{spont}(1mode) \cong 2h\nu BG_{max} \qquad (2.1.1\text{-}7)$$

where B = bandwidth, made equal to the homogeneous saturation bandwidth of the absorber. That is, if B is matched to the signal bandwidth, which in turn is determined by the pulse length, $\tau \cong 1/\pi B$, then the equivalent unpolarized spontaneous input is 2 photons per pulse.

If Eqs. (2.1.1-2, 3, 5, 6, and 7) are combined, the field-of-view through the BALAD receiver can be expressed as

$$\Omega_v \quad \frac{378hcs}{\pi\psi^2[dB]}\left[\frac{\alpha_o B}{I_s}\right]$$

or, in MKS units,

$$\Omega_v \quad \frac{7.60\times10^{-23}s}{[\alpha\lambda^2]\psi[dB]}\left[\frac{\alpha_o B}{I_s}\right] \quad . \qquad (2.1.1\text{-}8)$$

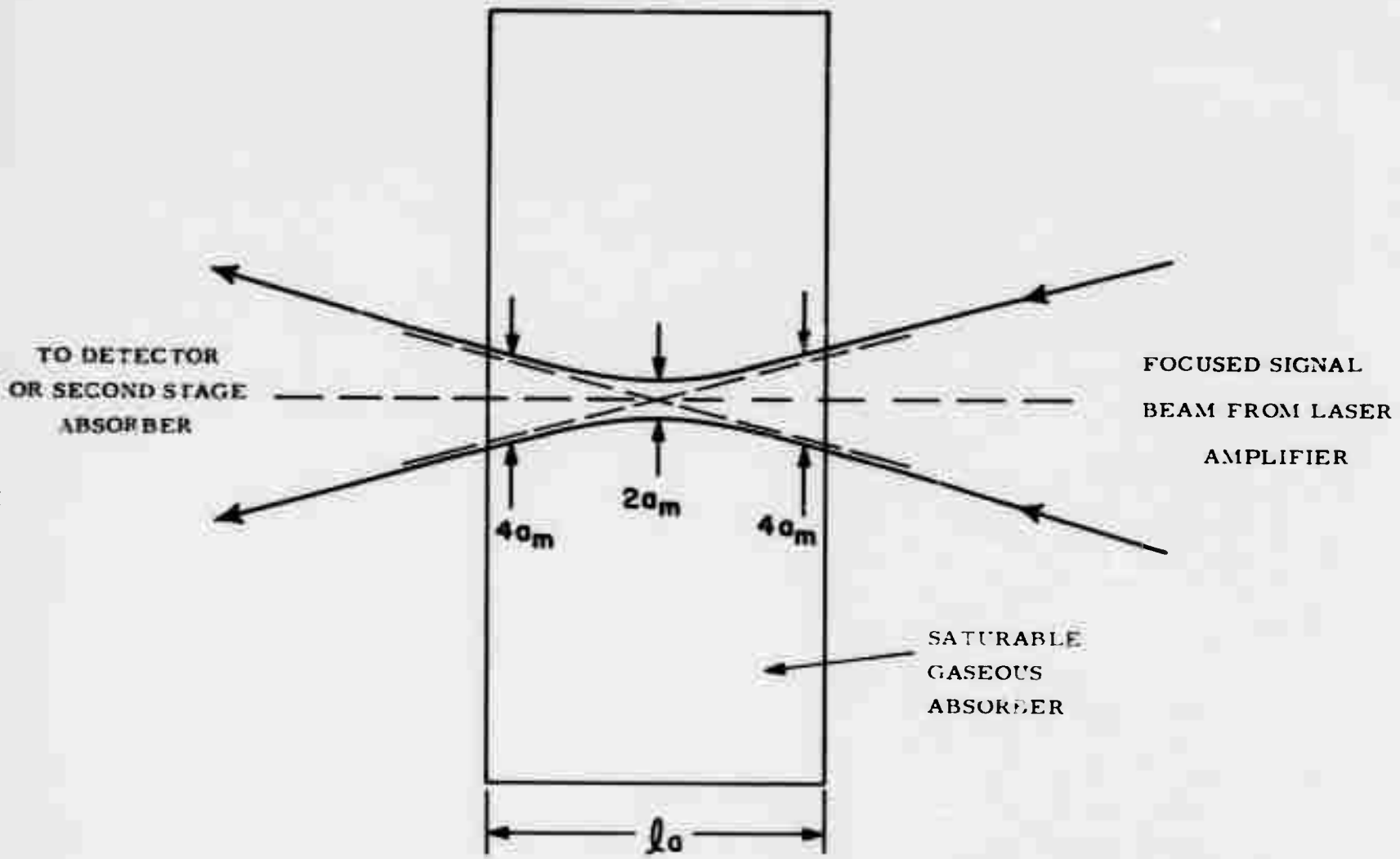

Fig. 4 - The "waist" shape of the extended focal spot is given by the confocal laser resonator theory if the signal beam is an undistorted plane wave.

The last bracket combines the absorber characteristics into a figure-of-merit:

$$F_M \equiv \left[\frac{\alpha_o B}{I_s}\right] \text{in meter/joule} \qquad (2.1.1\text{-}9)$$

as shown in Section 2.2.1, F_M is independent of the pressure. More precisely, for a passive absorber, F_M is independent of the collisional relaxation rate which determines the homogeneous bandwidth, B.

The bracket, $[\varphi\lambda^2]$ is characteristic of the laser medium. For CO_2, φ has been calculated to be usefully small: $\varphi(CO_2) = 0.03$.

The gain narrowing factor for spontaneous emission in the amplifier has been shown, for a Gaussian or Doppler line shape, to be[5]

$$\psi = \frac{\Delta\nu(\text{amplified spontaneous})}{\Delta\nu(\text{spontaneous})}$$

$$\cong \frac{1}{[L\alpha(\text{gain})]^{1/2}} = \left[\frac{4.34}{[dB(\text{gain})]}\right]^{1/2} . \qquad (2.1.1\text{-}10)$$

In practice,

$$[dB(\text{attenuation})] \approx [dB(\text{gain})] \approx 50dB . \qquad (2.1.1\text{-}11)$$

These approximations simplify expression (2.1.1-8) to:

$$\Omega_v = \frac{3.65 \times 10^{-23} s F_M}{[\varphi\lambda^2][dB]^{1/2}}$$

$$\cong \frac{5.16 \times 10^{-24} s F_M}{[\varphi\lambda^2]} . \qquad (2.1.1\text{-}12)$$

The field-of-view in steradians seen through the mirror collecting the input signal beam also depends on the aperture of the input optics (see Fig. 5). That is,

$$[\Omega_v \cdot \text{Area}]_{\substack{\text{laser} \\ \text{amplifier}}} = [\Omega_v \cdot \text{Area}]_{\substack{\text{input} \\ \text{mirror}}} . \qquad (2.1.1\text{-}13)$$

However, the number of modes or resolution elements seen through the system is independent of the input mirror aperture. That is the number of modes through any optical train which does not vignette the beam is:[6]

$$\begin{matrix}\text{Number of spatial modes} \\ \text{or resolution elements}\end{matrix} = m = \frac{\Omega_v}{\Delta\Omega(1 \text{ mode})} = \frac{\Omega_v \text{Area}}{\lambda^2} \qquad (2.1.1\text{-}14)$$

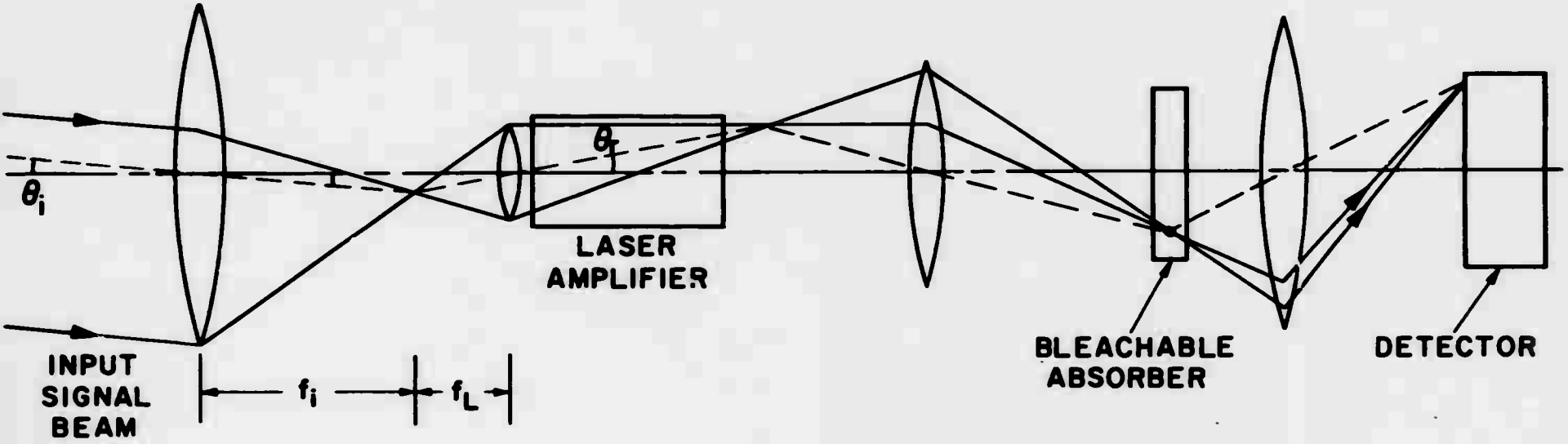

Fig. 5 - BALAD optics. Since $\theta_i f_i = \theta_L f_L$, the number of modes or resolution elements in the field-of-view, $m = \Omega_v \times \text{area}/\lambda^2$, is not altered by the input optics.

Therefore m is a more useful measure of the field-of-view than Ω_v:

$$m = \frac{4.05 \times 10^{-24} D^2 s F_M}{\varphi \lambda^4} \quad . \qquad (2.1.1\text{-}15)$$

It may be important to note that the number of resolution elements, m, is independent of the cross-sectional shape of the laser. In some applications, it may be useful to shape the cross-section of the field-of-view into a longer, thinner rectangle.

The other interesting quantities may likewise be expressed in terms of the important design parameters:

$$\begin{matrix}\text{maximum single-} \\ \text{stage gain factor}\end{matrix} = G_{max} = \frac{1.65 \times 10^{23} \lambda^2 [dB]}{s F_M} \quad . \qquad (2.1.1\text{-}16)$$

Incidentally, if a longer tube is needed to realize this gain than is allowed by Eq. (2.1.1-1), the beam can be refocused through several stages of amplification without altering the other quantities. Also:

$$P_{spont}(1 \text{ mode}) = \frac{0.0665 B \lambda [dB]}{s F_M} \text{ (in watts)} \qquad (2.1.1\text{-}17)$$

The signal power after emerging from the absorber will be approximately:

$$P_{signal}\Big|_{\substack{\text{out of} \\ \text{absorber}}} \approx 10 P_{spont}(1 \text{ mode}) \qquad (2.1.1\text{-}18)$$

If P_{spont}(1 mode) is multiplied by the number of spatial and spectral modes, we obtain the power which just saturates the amplifier. The maximum power to which the signal can be amplified by two or more complete BALAD stages is then:

$$P_{max}(\text{amplified signal}) \approx \frac{m \Delta\nu(amp)}{B} P_{spont}(1 \text{ mode}) \qquad (2.1.1\text{-}19)$$

also:

$$\text{focused spot radius} = a_m = \left[\frac{0.0212 \lambda [dB]}{s \alpha_o}\right]^{1/2} \qquad (2.1.1\text{-}20)$$

and[3]

$$\begin{matrix}\text{half-angle} \\ \text{of focused beam}\end{matrix} = \theta_{beam} = \frac{\lambda}{\pi a_m} = \frac{D}{f} \qquad (2.1.1\text{-}21)$$

where f = focal length of lens or mirror and finally:

$$\begin{matrix}\text{total absorber} \\ \text{path length}\end{matrix} = s'_a = \frac{0.231 [dB]}{\alpha_o} \quad . \qquad (2.1.1\text{-}22)$$

In Section 2.2.1, real absorbers are discussed and the figure-of-merit, F_M, is calculated from measured characteristics for several gases. Using F_M and the above equations, possible parameters for BALAD systems are calculated and tabulated in Section 2.2.2.

2.1.2. Optical Waveguide Configuration.

The optical waveguide configuration for the BALAD receiver is shown in Fig.2. This has several advantages over the "free focus" configuration depicted in Fig. 1-b:

(1) The need to refocus through a series of thin absorbers (or back-and-forth through a thin absorber) is eliminated. 100 or more absorbing stages may be collapsed into a bundle of gas filled tubes which might be 2 meters long (see Section 2.2.2).

(2) The insertion losses incurred by traversing a large number of optical interfaces will be eliminated. This factor directly multiplies the minimum detectable signal, as do factors (3) and (4) below.

(3) The constant diameter of the guide eliminates the geometrical intensity variation due to the varying cross-section in the waist of the focal spot. This reduces the attenuation of signal in the partially saturated absorber by several dB.

(4) The constant guide diameter also eliminates any extra signal attenuation due to transverse pulse spreading in the nonlinear absorber (see Section 2.2.4). This may amount to several dB.

(5) The constraint on spot size (Eq. 2.1.1-6) imposed by the need for adequate depth-of-focus is relieved. In effect, the number of stages, s, in the equations of Section 2.1.1 may be increased and the spot size decreased (Eq. 2.1.1-20). This allows a larger field-of-view through the amplifier (Eq. 2.1.1-12).

(6) It has been estimated that the mean free path of the absorbing molecules will approximately equal a guide diameter, $d \approx 100\mu m$, with relaxation times $T_1 \cong T_2 \cong 1\ \mu sec$. This will help ensure adequate cross-relaxation of the rotational levels. This, in turn, will ensure the saturation intensity will be the same for the signal and for the broad-band spontaneous emission, as has been assumed.

There will, of course, also be disadvantages inherent in the optical waveguide configuration.

(a) There will be an insertion loss on entering the absorber and exciting the desired mode. This factor multiplies the achievable field-of-view and may amount to a factor of 1/4, partially offsetting advantage (5).

(b) There will be attenuation in the walls and conversion to lossy modes. It is estimated below that this effect on the minimum detectable signal will be less than those noted in advantages 2, 3, and 4 above.

(c) It will be difficult to fabricate the bundle of waveguides. However, we believe it can be done with state-of-the-art techniques.[7] This is further discussed below.

The construction of a hollow 140μm diameter light pipe, which is coated by chemically deposited silver or gold would be a formidable task. Since glass and most other easily workable materials are opaque at 10μm, the coating must be deposited on the inside of the tubing. The difficulties which may be encountered are obvious. A more attractive procedure would be to deposit a thick silver coat on the outside of a smooth plastic or glass rod (or thin-walled tubing) which could then be dissolved away. Fifty meter long glass tubes with 100μm diameter have been drawn at Bell Telephone Laboratories.[7] There is no strong requirement for uniformity of diameter, but there is a stringent tolerance on circularity to prevent mode conversion. It is not known at present if this will be a serious problem. The appeal of this technique is that the inside surface of the resulting guide would be very smooth, even in relation to optical wavelengths. After the glass tubes are plated, they would be glued together in a straight array. The ends would then be ground flat and polished. Finally, the substrate tubing would be dissolved.

We now consider the losses associated with the propagation of an electromagnetic wave down a circular waveguide 140μm in diameter and 3 meters long.

The analysis of the modes of a circular waveguide is well known.[8]

The attenuation constant for the general $TM_{n\ell}$ mode at the frequency f is:

$$\alpha_{TM_{n\ell}} = \frac{R_s}{a\eta_1} \frac{1}{\sqrt{1 - (f_c/f)^2}}$$

where

$R_s = \sqrt{\frac{\pi f \mu}{\sigma}}$ = surface "skin" resistivity of guide wall

$\eta_1 = \sqrt{\frac{\mu_1}{\epsilon_1}}$ = impedance of the dielectric in the guide

a = guide radius

f_c = cutoff frequency of the mode.

For the $TE_{n\ell}$ modes,

$$\alpha_{TE_{n\ell}} = \alpha_{TM_{n\ell}} \left[\left(\frac{f_c}{f} \right)^2 + \frac{n^2}{(P'_{n\ell})^2 - n^2} \right]$$

where $P'_{n\ell}$ is the ℓ^{th} root of $J'_n(x) = 0$.

For $f >> f_c$, it is clear that the $TE_{o\ell}$ modes have much lower loss (by a factor $(f_c/f)^2$) than all other modes. In terms of practical numbers, for a lossless dielectric,

$$\eta_1 = \frac{377}{n} \text{ ohm} \qquad \text{where} \qquad n = \text{the index}$$

of refraction of the dielectric, and at 10.6μ, ($f = 3 \times 10^{13}$ Hz), $R_s = 1.4$ ohm. That is

$$\alpha_{TM} = \frac{1}{270a} = 53\,m^{-1} \quad \text{or} \quad 230\ dB/m \quad \text{for} \quad a = 70\mu .$$

For the TE_{11} mode, $(n^2/P'^2_{n\ell} - n^2) = 0.420$, so that all modes except the TE_{01} have large losses. For the TE_{01} mode, $\lambda_c = 1.64a = 115\mu$, so that at $\lambda = 10.6\mu$,

$$(f_c/f)^2 = (\lambda/\lambda_c)^2 = 0.0085$$

and,

$$\alpha_{TE_{01}} \doteq 0.45\,m^{-1} \doteq 2\,dB/m \quad .$$

As is well known, the anomolously low attenuation of the $TE_{o\ell}$ modes is due to the minimal currents which this mode induces in the waveguide walls. Any asymmetry in the guide or bending of the guide axis will produce currents in the walls which would directly increase losses. It would also generate other modes, which would be rapidly attenuated as we have discussed above. The tolerance on out-of-roundness would be about 0.3% to bring the conversion losses below the wall attenuation.[9]

From the geometry of the modes, it is clear that a plane-polarized plane wave incident on the end of the waveguide would couple dominantly to the TE_{11} mode. Coupling to the more desirable TE_{01} mode could be obtained by dividing the circular cross-section of the guide along a diameter parallel to the plane of polarization and introducing a 180° phase shift between the field incident on the two halves of the guide. This could be obtained by means of a thin dielectric film, with a thickness $(n-1)\lambda/2$ covering half of the guide. This can be accomplished more easily by orienting the incident plane wave at an angle

$$\theta = \tan^{-1} \frac{\lambda}{2a} \quad .$$

The proper angle would be about 4° without a stringent tolerance.

2.1.3. Fluctuations and Error Rates

The size of the minimum detectable signal pulse is determined by the required reliability of detection. Random fluctuations can cause an occasional signal pulse to fall below any arbitrary detection energy threshold and so be lost. Likewise, fluctuations in the background noise can occasionally exceed the threshold and produce a false signal. It has been shown that the relative shape of the pulse energy probability distribution curve is not greatly modified by unsaturated laser amplification except for the addition of spontaneous emission.[10] The input distribution is merely multiplied by the gain, G_{max}. Further, the detector will not add appreciable noise if the gain is sufficient. Thus, it is the fluctuations in the input pulse and in the spontaneous emission which determine the reliability of detection.

Fluctuations in the number of output photons per pulse can be caused by diffraction on passage through the turbulent atmosphere, by scintillation from a radar target, or they may be strictly statistical in nature. It will be assumed in this analysis that the error rates are dominated by the shot fluctuations in the number of photons per pulse, which set a lower limit. The fluctuations will then have approximately a Poisson distribution.[11] It is possible in some systems in principle to operate with a low signal-to-noise ratio, and to code and process the signal to achieve the required reliability. This is not possible with a BALAD receiver, since the signal level must be high enough to saturate the absorber and reduce the attenuation. However, it is shown below that the reliability of detection of single pulses increases very rapidly with average pulse energy. This, then, is the regime most appropriate for the BALAD receiver.

If the number of photons per pulse has a Poisson distribution, then the probability of an n-photon pulse is[12]

$$P_n = \frac{(\bar{n})^n e^{-\bar{n}}}{n!} \qquad (2.1.3\text{-}1)$$

where $\bar{n}$ is the average number. This is roughly a bell-shaped distribution curve. Well down on the tail on the low side, the probability of a pulse with no more than N photons is, to a sufficient approximation:

$$P_{n \not> N} = \sum_{n=0}^{N} \frac{(\bar{n})^n e^{-\bar{n}}}{n!} \cong \frac{(\bar{n})^N e^{-\bar{n}}}{N!} \quad . \qquad (2.1.3\text{-}2)$$

That is, the probability of a small N-photon pulse is greater than the sum of all still smaller pulses. This probability may be evaluated by using the Sterling approximation for the factorial:

$$N! \cong \sqrt{2\pi N}\ \left(\frac{N}{e}\right)^N \qquad (2.1.3\text{-}3)$$

whence,

$$P_{n \not< N} \cong \frac{1}{\sqrt{2\pi N}} \left(\frac{\bar{n}e}{N}\right)^N e^{-\bar{n}} \quad . \qquad (2.1.3\text{-}4)$$

For a simple numerical example, let $N = \bar{n}/e$ and $\bar{n} = 100$ photons/pulse, then the probability of a pulse not greater than N is

$$P_{n \not> N} = \frac{e^{-\bar{n}/3}}{\sqrt{2\pi\bar{n}/e}} \cong 10^{-16} \quad . \qquad (2.1.3\text{-}5)$$

The tolerably infrequent minimum pulse, N, cannot be made much larger than $\bar{n}/e$ without raising its probability to an intolerable level.

Similarly, we may ask for the probability that a noise pulse in a single spatial and spectral mode will be no less than N, and find the same expression (for $N \gg \bar{n}$):

$$P_{n \not< N} \cong \sum_{n=N}^{\infty} \frac{(\bar{n})^n e^{-\bar{n}}}{n!} \cong \frac{(\bar{n})^N e^{-\bar{n}}}{N!} \cong \frac{1}{\sqrt{2\pi N}} \left(\frac{\bar{n}e}{N}\right)^N e^{-\bar{n}} \quad . \qquad (2.1.3\text{-}6)$$

Consider a numerical example: let the spontaneous emission pulse be

$$N = \bar{n}e^3 \cong 20\bar{n} \qquad \text{and} \qquad \bar{n} = 2 \text{ photons} \quad .$$

In this case,

$$P_{n \not< N} < 10^{-80}(!) \quad .$$

This is approximately the case for a pulsed CO_2 amplifier (see Section 2.1.4).

It is obvious that arbitrarily low no-detection and false-detection error rates due to fluctuations can be achieved by setting the detection threshold sufficiently below the average signal and above the average noise pulses. However, an analysis of the effect of the absorber on the error rates is necessary before a quantitative criterion can be set.

In Section 2.1.1, it was noted that in the presence of a saturating signal, the absorption coefficient is reduced to (Eq. 2.1.1-4):

$$-\frac{1}{I}\frac{dI}{dz} \equiv \alpha = \frac{\alpha_o}{\sqrt{1 + I/I_s}} \quad .$$

This integrates approximately to

$$\sqrt{\frac{I_z}{I_s}} \cong \sqrt{\frac{I_o}{I_s}} - \frac{\alpha_o z}{2} \qquad (2.1.3\text{-}7)$$

in the regime where $I/I_s \gg 1$. Here,

I_s saturation intensity

I_z = intensity after propagating a distance, z, through the absorber.

I_o = intensity at $z = 0$.

Equation (2.1.3-7) gives rise to the nonlinear signal attenuation curve shown in Fig. 3. The nonlinear attenuation amplifies the relative size of fluctuations in the input pulse. This is shown by taking a finite differential of Eq. (2.1.3-7)

$$\frac{\Delta I_z}{I_z} \sim \frac{\Delta I_o}{I_o} \sqrt{\frac{I_o}{I_z}} \quad . \qquad (2.1.3\text{-}8)$$

This is really just a statement that the attenuation is larger for smaller pulses than for larger pulses. The effect is analogous to the operation of the "MARS" amplifier.[13]

There is no advantage to attenuation of the minimum detectable pulse below I_s as it emerges from the absorber. Therefore, it is reasonable to set the detection threshold at least equal to I_s. Thus, neglecting $I_z/I_s \sim 1$ in Eq. (2.1.3-7), we have

$$\left.\frac{I_o}{I_s}\right|_{min} = \left.\frac{E_o}{E_s}\right|_{min} \simeq \left(\frac{\alpha_o z}{2}\right)^2 \quad . \qquad (2.1.3\text{-}9)$$

Since $\alpha_o z$ is only a slowly varying function of the linear attenuation factor $\exp(-\alpha_o z)$, a value can be given for the minimum detectable input pulse energy ratio, E_o/E_s, which is adequate for any reasonable operating conditions. The required background attenuation is ≈ 50dB (approximately equal to the laser gain). Therefore,

$$\left.E_o/E_s\right|_{min} \simeq 25 \qquad (2.1.3\text{-}10)$$

and

$$\left.E_o\right|_{min} \simeq 50 \text{ photons/pulse}$$

If E_s = 2 photons/pulse. E_o must be multiplied by the insertion loss factor (see Section 2.1.2). Any smaller pulse such as the example after Eq. (2.1.3-6) will be more attenuated and not detected.

The pulse input to the amplifier is actually the sum of the signal pulse and the spontaneous pulse coherent with the signal. If these are out-of-phase some cancellation would result. However, the probability of substantial reduction is even less likely than the probability of the minimum detectable signal. In this connection, we may note that at the input the signal will power broaden the absorber and allow more spontaneous emission to enter the saturated spectral slot. However, at the exit of a minimum detectable signal, the slot has narrowed to the signal bandwidth. We thus conclude that, for a signal pulse rate of 10^6/sec and average signal input of 150 photons/pulse, the no-detection error rate due to Gaussian fluctuations would be less than 1/(100 years).

The false detection rate due to statistical fluctuations may flow from either of two sources:

(a) a large noise fluctuation in a single mode.

(b) a fluctuation in total average power in all modes, which is exponentially attenuated in the absorber.

The rate for case (a) is the probability of a single detectable pulse multiplied by the "opportunity rate." The latter is the product of the rate per mode, B, the number of spatial modes in the field-of-view, and the amplifier to signal bandwidth ratio:

$$\text{False detection rate for all single modes} \cong [P_{n \neq N}]m(\pi B)\left[\frac{\text{gain width}}{B}\right] \quad . \qquad (2.1.3\text{-}11)$$

For parametric values which give a tolerable no-detection rate this false detection rate is immeasurably small. Thus, the detection threshold for an acceptable no-detection rate also ensures no false detection.

At the amplifier input, the total amount of spontaneous emission in all modes during a signal pulse length is:

$$\text{total } \bar{n}_{sp} = [\bar{n}_{sp}(\text{single mode pulse})]m\left[\frac{\text{gain width}}{B}\right] \quad . \qquad (2.1.3\text{-}12)$$

If the post-amplifier bandwidth is limited to B, the effective $\bar{n}$ for computing statistical fluctuations is reduced to

$$\bar{n}_{sp} = [\bar{n}_{sp}(\text{single mode pulse})]m\left[\frac{\text{gain width}}{B}\right]^{1/2} \quad . \qquad (2.1.3\text{-}13)$$

For a CO_2 amplifier $\bar{n}_{sp}$ (single mode pulse) $\approx$ 2 photons. Thus typically, $\bar{n}_{sp} \approx 10^5$. A fluctuation equal to this is already highly unlikely. $\bar{n}_{sp}$ is spread over all modes and

enters the absorber at saturation level. To avoid false detection, the total spontaneous pulse must be attenuated below the signal detection threshold as it exits the absorber – i.e., ~ -50dB.

2.1.4. Maximum Gain of a Laser Amplifier

Expression (2.1.1-2) gives the maximum gain achievable without saturating a laser amplifier. This may be readily obtained by extending Yariv's derivation of the amplified unpolarized spontaneous emission power:[14]

$$P(\text{amp. spont.}) \cong 2h\nu\Delta\nu_{sp} KG\left[\frac{\Omega_v}{\lambda^2/A}\right] \qquad (2.1.4\text{-}1)$$

where the following have been defined in Equations 2.1.1-10 and 2.1.1-14):

$\Delta\nu_{sp} = \psi\Delta\nu_{Dop}$ = narrowed amplified spontaneous emission bandwidth

$\left[\frac{\Omega_v}{\lambda^2/A}\right]$ = no. of spatial modes in field-of-view

$K \equiv \frac{N_2}{N_2 - N_1(g_1/g_2)}$ = ratio of upper level population to population excess

$g_1/g_2 \approx 1$ = statistical weight ratio for a CO_2 laser.

K is proportional to the spontaneous emission power per unit gain coefficient. Any background thermal radiation is neglected in comparison with spontaneous emission. For a CW CO_2 laser,[15] $\alpha_G \cong$ 5dB/meter and $K \cong 2.2$. For a pulsed CO_2 laser,[16] $\alpha_G \cong$ 13dB/meter and $K \cong 1.2$. K is usually close to 1 and in most cases is neglected. From Eq. (2.1.4-1), the output intensity is

$$I(\text{amp. spont.}) = 2h\nu\Delta\nu_D\psi KG\frac{\Omega_v}{\lambda^2} \quad . \qquad (2.1.4\text{-}2)$$

On the other hand, the saturation intensity for a homogeneously broadened line is[17]

$$I_s = \frac{8\pi h\nu\Delta\nu_{homo}}{\varphi\lambda^2} \qquad (2.1.4\text{-}3)$$

where

$\Delta\nu_{homo} \cong \Delta\nu_{Doppler}$ for the CO_2 amplifier.

φ = "branching ratio" for the laser transition.

It has been assumed that all the rotational levels are cross-relaxed by collisions during the pulse duration. Hence, all these levels must be saturated when

the laser pair is saturated. We have calculated that the rotational group contains about 30 times the population of the laser pair. (See Final Report.) Therefore, for CO_2, $\varphi \cong 1/30$.

If the amplified spontaneous emission is set equal to the saturation intensity at the ends of the amplifier, we may solve for the maximum unsaturated gain,

$$G_{max} = \frac{4\pi}{\varphi \Psi K \Omega_v} \quad . \qquad (2.1.4\text{-}4)$$

For $K \approx 1$, this is the result stated in Equation 2.1.1-2.

2.1.5. Key Assumptions

In this section, the key assumptions made in modeling the BALAD receiver have been collected to give the reader a "feel" for the validity of the conclusions.

CW rate equations have been used for both absorber and amplifier calculations even though pulsed signals are contemplated. It is known that, when the relaxation times, T_1 and T_2, are comparable to the pulse duration, propagation through a saturated absorber distorts the pulse spatially and spectrally and alters the attenuation. Any spreading of the focused pulse will increase the minimum detectable input pulse energy. These effects can be calculated using the field equations and the quantum Block equations for the medium. However, when the model is made realistic the equations become too complex to solve analytically. Such a model would, for example, take account of the inhomogeneity of the absorber transition and the degeneracy of the molecular rotational levels. The equations have been solved numerically for some fairly realistic cases, but unequivocal conclusions cannot yet be drawn. These computations will be discussed in the final report. A tentative conclusion is that the effects will be largely washed out in highly degenerate media since each substate presents a slightly different dipole moment to the passing wave.

Propagation through the atmosphere has not been taken into account, nor has target scintillation. To the extent that fluctuations larger than Gaussian are introduced, the average signal pulse would have to be increased.

The Pulse Bandwidth of the signal has been assumed to be given by $B = 1/\pi\tau$, where τ = pulse duration. If the spectral width is broadened, then the minimum detectable pulse energy would be correspondingly increased. Such broadening might be caused by target rotation or by chirping or other coding of the transmitted pulses.

Power Broadening of the saturated bandwidth in the absorber occurs: $\Delta\nu_1 = \Delta\nu_s \sqrt{1 + I/I_s}$. As already discussed in Section 2.1.3, this would let more spontaneous emission through if the signal pulse excited the absorber with higher than minimum

energy. However, the minimum detectable is set to leave the absorber without so broadening the spectral slot. It is expected that there will also be a spatial power broadening of saturated focal spot. This effect has not been analyzed, but again it would not occur with the minimum detectable signal.

Insertion Losses have been briefly discussed in Section 2.1.2, but have not been explicitly taken into account in the design. These losses have several different kinds of consequences:

(a) Those losses which occur within the amplifier have no effect since both signal and noise are equally attenuated and can be compensated with longer amplifier. Such a loss might occur in a filter used to eliminate the other CO_2 lines.

(b) Those losses occurring between amplifier and absorber have the effect of reducing the field-of-view since a higher net gain would then be required to bring the spontaneous emission up to the saturation intensity. This might amount to a factor of 4 in the case of the optical wave-guide configuration and somewhat reduce its advantage.

(c) Those losses occurring within the absorbing train would have the effect of increasing the minimum detectable input signal. This is because the signal would be differentially more affected than the spontaneous emission. Such losses might amount to a factor of 4 or more on either configuration. However, they could be countered, if desired, by inserting short amplifier sections within the absorber train.

(d) Losses occurring after the absorber have no effect. Thus, noisy or inefficient signal processing or detection can be used. For example, heterodyne Doppler detection could be used without requiring separate post detector amplifiers for each spatial and spectral mode.

The laser level population factor, $N_2/(N_2 - N_1) \approx 1$, has been assumed. A factor different from 1 would increase the spontaneous emission and decrease the maximum gain, G_{max}. Published reports suggest that this is nearly so for a pulsed (500 usec) CO_2 amplifier. It is generally assumed to be so for other gas lasers in their best transitions under optimal operating conditions. (E.g. xenon at $\lambda = 3.5$ um.)

The relaxation times, T_1 and T_2, need not have any assumed relation to each other in these calculations, since we are using measured rather than calculated absorber characteristics for the figure-of-merit, F_m. However, it has been assumed that the saturation intensity, I_s, is unchanged by the presence of just-saturating broadband spontaneous emission. This amounts to assuming that the cross-relaxation rate between rotational levels is the same as between different velocity (Doppler) groups within one rotational level. Our measurements as a function of pressure imply that this is so within a factor of 2.

2.2. Real Absorbers and BALAD Characteristics

Task 4.1.1 of the contract calls for "Investigation of saturable (gaseous) absorbers with a view towards receiver application and development of narrow band spatial and spectral filters. This is to be accomplished by screening of available 10.6μm Q-switchable bleachable absorbers and other materials suitable for 3-5μ, with subsequent measurement and analysis of the following properties as a function of pressure, temperature, and isotopic composition (where relevant):

(1) absorption
(2) saturation
(3) relaxation rates (bandwidth)
(4) line centers and shapes relative to 10.6μm and 3-5μm laser lines."

The above listed key properties determine the suitability of a given gas for use in a BALAD receiver.

The results of Task 4.1.1 are summarized in Section 2.2.1 below. An extended discussion of the theory, experimental procedures and results will be contained in the final report. In Section 2.2.2, characteristics of BALAD receivers using the best absorbers are summarized. Essentially, useful receivers are feasible at 10.6 and 3.5μm, insofar as this can be determined without actually testing such receivers. In Section 2.2.2, it is recommended that such a test be made during 1972 using the economical xenon amplifier and absorber.

2.2.1. Absorber Characteristics

In Section 2.1.1, it was shown that the above listed key absorber properties can be combined in a figure-of-merit:

$$F_M \equiv \left[\frac{\alpha_o B}{I_s}\right] \quad . \qquad (2.1.1\text{-}9)$$

F_M limits the achievable field-of-view through the receiver. The absorption coefficient, α_o, the homogeneous saturation bandwidth, B, and the saturation intensity, I_s, cannot be accurately calculated. Therefore, they must be measured for the most promising gases.

A list of 71 molecular gases known to have absorption bands in the region of the CO_2 laser lines has been compiled from the literature. An additional 4 molecules are known to absorb near the high gain laser lines in the 3-5 μm region (He-Ne @ λ = 3.39μm and He-Xe at 3.5μm). For 19 of these an overlap of at least 1 CO_2 laser line has been established. No absorbers overlapping the CO laser line in the 4-5μm region have yet

been investigated, though it is believed that there is an excellent chance that a good absorber can be found.

Average absorption coefficients have been measured for those with an overlap. Finally, for the two best absorbers, (SF_6 and SiF_4), the degree of overlap, the spectral shape of the absorption curve, the saturation intensity, and the saturation bandwidth were measured as a function of pressure. The temperature coefficient of the absorption coefficient was measured for that line which overlapped the CO_2(P16) line. In addition, the key absorption characteristics of overdriven xenon gas at $\lambda = 3.5\mu m$ were measured as functions of pressure and current density. These values are listed in Table 2.2.1-1 together with those for CO_2 itself. Obviously, the latter two absorbers are a perfect match for the corresponding amplifiers. These values were used to calculate the receiver characteristics presented in Table 2.2.2-1.

Table 2.2.2-1

Key Characteristics of Bleachable Absorbers in BALAD Receivers

Gas	Absorption Coefficient, α_o	Homogeneous Saturation Bandwidth, B	Saturation Intensity, I_s	Figure-of-Merit $F_M \equiv [\frac{\alpha_o B}{I_s}]$
CO_2	$0.7 \frac{(\text{meter})^{-1}}{\text{torr}}$	$7 \times 10^6 \frac{\text{hertz}}{\text{torr}}$	$5 \times 10^4 \frac{\text{watts}}{\text{m}^2\text{torr}^2}$	$1.0 \times 10^2 \frac{\text{meter}}{\text{joule}}$
SiF_4[a]	30	5×10^6	3.5×10^4	4.2×10^3
SF_6(300 °K)[b]	130	21×10^6	7×10^4	3.9×10^4
SF_6(130 °K)[b]				3.1×10^5
Xe(discharge)[c]	$(6.9\ \text{m}^{-1})$[c]	$(7 \times 10^6\ \text{hertz})$[c]	$(0.9 \frac{\text{watts}}{\text{meter}^2})$[c]	5.4×10^7

a. coincidence with the P-36 line of the 9.6μm CO_2 group.

b. coincidence with the P-16 line of the 10.6μm CO_2 group. The vapor pressure at 130 °K is approximately 0.05 torr.

c. The values for the xenon 3.5μm transition are for a 400 ma/cm^2 discharge, 1 cm diameter, 0.05 torr pressure. Hence, only its figure-of-merit can be directly compared with the other gases.

Two quite different types of absorbers are represented in Table (2.1.1-1). The molecular transitions are between rotational levels in two vibrational state of the ground electronic state. These are passive, resonance transitions in the sense that the lower level is populated at room temperature (or, in the case of CO_2, at a slightly elevated temperature). In the case of xenon the absorbing transition (the same as the laser transition) is between two different electronic states populated by excitation in a discharge. Both have advantages and disadvantages as potential absorbers. They will be discussed in detail in the final report. The salient points are summarized below.

The molecular electronic states (those with distinct electron configurations) are subdivided into many vibrational and rotational states. Thus, in the linear CO_2 molecule each vibrational state has about 30 distinct populated rotational substates, while the spherical SF_6 has over 1000 such substates. Thus, if vibration bands overlap, there is an excellent chance of overlap of particular rotational transitions. In fact, most of the CO_2 laser transitions are overlapped by one or more SF_6 absorbing transitions. On the other hand, the multiplicity of atomic transitions is much smaller and the chance of an overlap is smaller (~1%). Nevertheless, because these transitions make superior absorbers, we intend in the future to make a computer search among the feasible candidates for overlap of a good CO_2 transition. Of course, if the same transition can be both a good amplifier and a good absorber, under different conditions, the problem is solved. Such is the case for the xenon transition at $\lambda = 3.51\mu m$.

The price to be paid for a good chance of adequate overlap is that the population is divided among many rotational levels and any one absorption coefficient is correspondingly reduced. A reasonably good absorption coefficient is possible only if the lower rotational level is in the lowest vibrational state.

It is not accidental that vibrational energy level differences generally are of the same order as the CO_2 laser photon energies, since the CO_2 laser transition are between 2 such vibrational levels. On the other hand, atomic transitions of the order of $\lambda \sim 10\mu m$ are usually between electronic states of high energy. The lower level must be populated by collisions in a discharge. Thus, there is population penalty in the atomic case also. The absorption coefficient is reduced by something like the Boltzmann factor. Table (2.2.1-1) shows similar absorption coefficients for SF_6 and xenon despite a much stronger xenon transition. However, the corresponding saturation intensity, $I_s(Xe)$ is much smaller and results in a higher figure-of-merit.

Both the absorption coefficient, α_o, and the inverse of the saturation intensity, $1/I_s$, are proportional to the square of the transition dipole moment, $\langle \chi \rangle$. Therefore, the figure-of-merit,

$$F_M = \left[\frac{\alpha_o B}{I_s}\right] \propto \langle\chi\rangle^n \text{, where } n \geq 4 \qquad (2.2.1\text{-}1)$$

and is very sensitive to $\langle\chi\rangle$.

For a transition between vibrational states within the same electronic state, the electric dipole moment would be zero were it not for the small charge motions in the molecule due to the vibration. Thus, the strength of these transition, $\langle\chi\rangle^2$, is 10^{-4} or less of an allowed atomic transition such as the xenon 3.51μm transition.

One may ask if a stronger molecular absorber than SF_6 is likely to be found in the 10.6μm region. The existing theory is not able to accurately predict the strength of particular vibrational transitions. However, a review containing a table of 160 measured total vibrational band strengths associated with some 52 different molecular bonds shows the SF_6 band at 10.6μm to be close to the strongest.[18] Fortunately, it is good enough to allow a useful field-of-view through a BALAD receiver.

2.2.2. Achievable BALAD Receivers

Using the figures-of-merit for SF_6 and Xe in Table (2.2.1-1) and the known properties of CO_2 and Xe amplifiers, it is possible to compute sets of BALAD receiver characteristics using the equations of Section 2.1. Examples of such sets are presented in Table (2.2.2-1).

The CO_2-SF_6 BALAD receiver size is dominated by the amplifier. This follows from the relative low gain of the CO_2 laser medium. A moderate folded length for the receiver, as compared with the transmitter of a long range radar, is made possible by the 10 dB/meter gain of a pulsed amplifier. Use of the optical wave guide configuration brings the size of the absorber down to a 2 meter length and an overall diameter of 1 centimeter for the waveguide bundle.

The 4000 resolution element field-of-view is not large but it should be compared with the optical heterodyne detector array required for a similar performance: 4000 detectors with a total of 400,000 independent post-detector amplifiers for the spectral slots. The field-of-view can be increased in direct proportion to the (folded) length of the absorber.

With a second stage of amplification the peak signal power is brought up to a respectable 0.2 watt. This, in turn, makes possible a heterodyne Doppler measurement without requiring an array of detectors and circuits. If a weak local oscillator is used, a negligible amount of noise will be introduced. This would be accomplished by inverting the power ratio of signal and local oscillator – that is, by interchanging their roles in the heterodyne detection process.

Table 2.2.2-1

BALAD Receiver Characteristics

	CO_2 laser-P(16) line at 10.6μm SF_6 absorber at 130°K Figure-of-Merit, $F_M = 3 \times 10^5$ m/j	Xenon laser at 3.5μm Xenon discharge absorber Figure-of-Merit, $F_M = 5 \times 10^7$ m/j
input signal pulse	150 photons (x2 for insertion loss)	150 photons
pulse length	0.3 microseconds	0.3μsec
input signal power	2×10^{-11} watt	3×10^{-11} watt
pulse bandwidth	1 MHz	1 MHz
amplification bandwidth (signal frequency range)	10 MHz	30 MHz
field-of-view	60 x 60 resolution elements	25 x 25 resolution elements
(signal direction range)	(0.4 deg. x 0.4 deg.)	(0.5 deg. x 0.5 deg.)
pulse error rates no-detection rate	10^{-16}/pulse	10^{-16}/pulse
false alarm rate	<< 1/year	<< 1/year
Max. signal amplification		
(first stage)	70 dB	60 dB
(second stage)	30 dB	20 dB
Max. peak signal to detector (2 stages)	0.2 watt	0.003 watt
relative background attenuation	50 dB	50 dB
effective quantum efficiency	> 90%	> 90%
unfolded pulsed amplifier length		
(first stage)	7 meters	1 meter
(second stage)	2 meters	0.5 meter
amplifier diameter	10 cm	1 cm
no. of absorber stages (free focus - see Fig. 1)	100 stages	1 stage
absorber path length	2 meter	2 meter
optical waveguide length (see Fig. 2)	2 meter	
focused spot diameter	0.22 mm	2 mm

As was noted in Section 2.1.3, the detection error rates are primarily determined by the input pulse statistics and are little affected by other considerations. In effect, the quantum efficiency of the receiver is close to 100%.

The Xe-Xe BALAD receiver outlined in Table (2.2.1-1) is the design which can be readily and economically tested during 1972. The advantage is that only a single stage of absorption is necessary to obtain a field-of-view large enough to make a good experimental test of the predicted receiver characteristics. On the other hand, several hundred stages of refocusing to a smaller spot size could increase the field-of-view to a substantial 400 x 400 resolution elements. This would be equivalent to television picture resolution. A compact and economical configuration for accomplishing this without increasing the overall length is being worked out and will be presented in future reports.

The 1 watt of average power which is presently available at $\lambda = 3.5\mu m$ does not allow a range comparable to a CO_2 laser radar.[19] However, shorter range but higher resolution radars are possible, as well as, long range optical communication systems with relaxed aiming requirements.

REFERENCES

1. G. Gould, Proposal to ARPA, "Investigation of Low Noise Laser Receiver", April 1969.

2. A. Yariv, "Quantum Electronics," p. 267 (New York: John Wiley & Sons, Inc.) 1968.

3. Ibid., p. 224, et seq.

4. Ibid., p. 415

5. Ibid., p. 292

6. Ibid., p. 35

7. J. Stone, IEEE J. Quant. Electr. QE-8, 386 (1972).

8. Ramo and Whinnery, "Fields and Waves in Modern Radio," (New York: John Wiley & Sons, Inc.) 1944.

9. S.E. Miller, Bell Syst. Tech. Journ. 33, 1209 (1954).

10. H. Steinberg, Proc. IEEE 51, 943 (1963).

11. M.O. Scully and M. Sargent, III, Physics Today 25, Feb. 1972, p. 45.

12. "Handbook of Mathematical Functions," N.B.S. Applied Math. Series (No. 55), U.S. Dept. of Commerce, Chapt. 26.

13. B. Senitzky and S. Cutler, "Amplification by Resonance Saturation in Millimeter Wave Cavities," Microwave Journal, Jan. 1964.

14. A. Yariv, "Quantum Electronics," p. 414 (New York: John Wiley & Sons, Inc.) 1968.

15. Djeu, Kam, and Wolga, IEEE J. Quant. Electr. QE-4, 256 (1968).

16. Smith and Forster, IEEE J. Quant. Electr. QE-4, 348 (1968).

17. A. Yariv, "Quantum Electronics," p. 266 (New York: John Wiley & Sons, Inc.) 1968.

18. L. Gibov & V. Smirnov, Sov. Phys. Uspekhi 4, 919 (1962).

19. R. Targ & M.W. Sasnett, J. Quant. Elect. QE-8, 166 (1972).